Effect of Sudden Pressure on Spinal Cord and Break Down (Dura Mater, Arachnoid Mater and Pia Mater) an Experimental Analysis on Threshold Levels

R. Derakhshan, M.T. Ahmadian*

[1] School of Mechanical Engineering, Sharif University of Technology, Tehran, Iran.
Email: derakhshanhoore_reza@mech.sharif.edu, rzdrksn@gmail.com

[2] School of Mechanical Engineering, Sharif University of Technology, Center of Excellence in Design, Robotic and Automation, Tehran, Iran.
Postal code: 145888-9496
Phone: (+98) 21 - 66165503
FAX: (+98) 21 – 66000021
Email: ahmadian@sharif.edu

Abstract

Spinal cord is enveloped by three layers of meninges to protect the central nervous system from mechanical damage. Surgical operation and resection of tumors in the vicinity of spinal cord is complicated and risky because exposes it to probable irreversible damage. Nowadays, to reduce the risk of these operations, attempt is made to remove tumor using safer technique such as waterjet operation. In these methods interaction of waterjet and spinal cord is inevitable. To have safe interaction of operation, a standard development of waterjet criteria is necessary. In the present study a system of waterjet is designed for surgical operation in the vicinity of spinal cord along with limitations and thresholds. For this purpose, spinal cords of 2 years old sheep are considered. Results show that meninges layer is stiff enough to protect sheep spinal cord from rupture for pressures up to 8 bar. The role of different meninges layers to protect internal spinal cord soft tissue in interaction with waterjet is also studied. Effects of angle between nozzle and spinal cord axis, liquid density, nozzle diameter and waterjet velocity on internal soft tissue degradation as well as spread of inky waterjet beneath Arachnoid mater is also investigated in the absence of dura mater.

Keywords: Spinal Cord, Medical Operation, Experimental Test, Operation Threshold, Sheep, Meninges Layer, Dura Mater, Waterjet.

1. Introduction

The primary function of the spinal cord is to transmit nerve signals from the motor cortex to the body and from the afferent fibers of sensory neurons to the sensory cortex. It also serves as a center for coordinating numerous reflexes. The spinal cord contains reflex arcs that can independently control reflex actions [1]. Additionally, it consists of groups of spinal interneurons that form neural circuits known as central pattern generators. These circuits regulate motor commands for rhythmic movements such as walking. When viewed in cross-section, the spinal cord displays white and gray matter tissues. The peripheral region contains white matter tracts comprising ascending and descending myelinated fibers, which house both sensory and motor axons. The central region, characterized by its butterfly shape, consists of gray matter cells that are unmyelinated. Running through the middle is a central canal that contains cerebrospinal fluid, which circulates to the brain's ventricles [2].

The meninges consist of three membranes that surround and separate the brain and spinal cord from the bony walls of the skull and spine. Depending on their location, they are referred to as the cranial meninges, which enclose the brain, and the spinal meninges, which encase the spinal cord. Nevertheless, the cranial and spinal meninges are continuous and composed of the same layers. The meninges are named, from outermost to innermost, as follows: Dura mater, Arachnoid mater, and Pia mater. The Dura mater is the outermost and toughest layer, made of dense fibrous tissue that provides significant protection. It is the only meningeal layer that is sensitive to pain. The Arachnoid mater is the middle layer, characterized by its cobweb-like pattern formed by elastic tissue and collagen. The cerebrospinal fluid flows beneath the arachnoid mater in the subarachnoid space, situated above the pia mater. The Pia mater is the innermost layer, tightly adhering to and surrounding the spinal cord and brain. Unlike the loosely fitting arachnoid and dura mater, the pia mater forms a close attachment. Among the three meningeal layers, the pia mater is the thinnest and most delicate. These layers define three clinically significant potential spaces: the epidural space, the subdural space, and the subarachnoid space. The meninges serve several functions, including protecting the brain and spinal cord against mechanical trauma, providing support for blood vessels, and creating a continuous cavity for the passage of cerebrospinal fluid (CSF) [2,3]. Additionally, the meninges also cover the optic nerve, located at the frontal base of the skull [4].

In addition, it is noteworthy that the resection of tumors in the vicinity of the spinal cord is complicated and risky because the margins between intramedullary tumors and the normal tissues of the spinal cord are often unclear [5]. The removal of skull base tumors, which are located near the optic and olfactory nerves, can expose them to irreparable complications. Recently, Ogawa et al. investigated a new technique for removing pituitary tumors in the skull base region [6]. This technique utilizes the pulsed laser-induced liquid jet (LILJ) system, which efficiently and safely removes the tumor without damaging blood vessels and nerves. Furthermore, a study by Nakagawa et al. in 2015 examined the safety of the LILJ system and concluded that the waterjet is a safe method for removing lesions on the pituitary gland and its surrounding area [7]. Endo et al. utilized an actuator-driven pulsed waterjet to resect cavernous malformations of the brain and spinal cord [8]. In these instruments, MEMS devices enhance the functionality, performance and accuracy of waterjet systems. Leveraging MEMS technology makes it possible to miniaturize and make waterjet systems more portable [9]. Nowadays, more attempts are being made to reduce the risk of surgery and remove tumors using liquid-based techniques.

Alamoud et al. demonstrated the use of continuous and pulsed waterjet for pituitary surgery and highlighted its advantages over other methods [10]. Kok et al. investigated the safety and potential benefits of water jet drilling compared to conventional microfracture awls, assessing side effects and perioperative complications. Their findings concluded that water jet drilling provides adequate fibrocartilage repair tissue [11]. Babaiasl et al. conducted research on the depth of cut of a waterjet in soft tissue for medical applications using finite element method simulation and experimental tests with steerable needles [12-13]. Babaiasl also proposed an application of waterjet technology in the medical field, specifically waterjet cutting at the tip of a steerable needle [14]. Moradiafrapoli et al. designed an experimental study to demonstrate the hydrodynamic performance and starting phase of waterjet for needle injection. They used gel as a soft tissue with varying densities in the water jet. This study also investigated the dependence of waterjet parameters on fluid density [15]. Kraaij et al. described the requirements for a waterjet application in interface tissue removal for percutaneous hip fixation techniques. They presented an interface tissue removal applicator that reduces the risk of water pressure build-up [16]. Liu et al. investigated the feasibility of high-pressure waterjet drilling as a novel technique for enamel drilling [17]. Abdou et al. conducted an experimental test to determine the optimal waterjet pressure needed to cut and drill skin layers without damaging other organs [18]. Previous studies have not explored the applicability of waterjet in spinal cord surgery, nor have they established a standard threshold for a safe medical operation using waterjet interaction with the spinal cord. Derakhshan et al. used waterjet with different diameter to interact dura matter as stiffest layer of meninges. They show that this layer has enough durability to protect spinal cord against rupture up to 8 bar pressure [19].

In the present study, a waterjet system is designed to perform spinal cord. Ensuring the safety of waterjet characteristics is crucial to minimize treatment risks, particularly in proximity to vulnerable organs like the spinal cord and optic nerves. The interaction between the waterjet and the spinal cord, as well as the different meningeal layers, is being investigated to determine threshold characteristics for a safe surgical procedure. Additionally, the effect of waterjet fluid density on the failure criteria of spinal cord surgery is being studied.

2. Material & Methods

2.1. The waterjet apparatus

A waterjet instrument is designed with various nozzle diameters (0.2, 0.3, 0.4, 0.5 mm) to offer different ranges of waterjet caliber. A control system is implemented to maintain a constant pressure throughout the test. The system is controlled by a microcontroller programmed in C++ that regulates the desired pressure and controls the solenoid valve (Figure 1). Depending on the difference between the gauge pressure and the desired pressure, the appropriate on-off signal is sent to the relay coil, which acts as the actuator for the air compressor. As a result, the output speed of the waterjet remains consistent and stable during the test.

2.2. Waterjet velocity calibration

The velocity of the water jet can be calculated using Bernoulli's Law, assuming negligible energy loss. Eq.1 provides the pressure difference between point 1 and point 2:

$$\frac{1}{2}\rho V_1^{\,2} + P_1 + \rho g h_1 = \frac{1}{2}\rho V_2^{\,2} + P_2 + \rho g h_2 \qquad (1)$$

In this equation, V, P, ρ and h are velocity, pressure, density and height. Point 1 and 2 are considered to be in the tank and at the exit of the waterjet respectively. In this system h_1 and h_2 are almost at the same level and V_1, P_2 may be equal to zero. So, Eq.1 can be simplified as Eq.2:

$$P_1 = \frac{1}{2}\rho V_2^{\,2} \qquad (2)$$

Due to the fact that considerable energy is lost within the micron caliber nozzle, the velocity of the water jet versus pressure is measured and shown in Figure 2-a. Waterjet velocity is measured by dividing the volumetric flow rate (Q) by the nozzle area (A). The volumetric flow rate is also calculated by the ratio of fluid (Vf) to the time (t) that the waterjet passes through the nozzle (Q=Vf/t). This relationship can be represented by the regression equations in Table 1. It should be noted that according to Eq.2, the waterjet velocity is the same for all nozzles and is independent of the nozzle caliber.

Figure 2-b also shows the calibrated waterjet velocity versus gauge pressure for saturated saltwater (room temperature, NaCl, pressure ≅1 atm), and its regression equations are given in Table 2.

The density of NaCl is 2.17 g/ml and its maximum solubility at 25 $C^{\circ}$is 357 mg/ml of water. Therefore, the density of saturated salt water at room temperature is 1.165 g/ml [20]. The volumetric flow rate (Q) of the water jet versus pressure for pure and salt water are shown in Figure 2-c and Figure 2-d. It could be calculated by multiplying the liquid velocity by the nozzle cross section (Q=V*A).

In the interaction of the water jet with the material, the mass flow rate plays a key role, which can be obtained from Eq. 3.

$$\dot{m} = \frac{dm}{dt} = \rho Q = \rho v A \qquad (3)$$

In Figure 2-c and Figure 2-d, it can be observed that, for the same tank pressure and nozzle diameter, the waterjet output velocity (volumetric flow rate) is higher for pure water compared to saltwater. Conversely, saltwater is denser than pure water. Therefore, to facilitate better understanding and comparison, Figure 2-e and Figure 2-f present the waterjet mass flow rate for pure water and saltwater in relation to tank pressure. These figures demonstrate that the mass flow rate for saltwater exceeds that of pure water at the same tank pressure and nozzle diameter.

2.3. Experiments

Test 1:

This test examines the effects of nozzle diameter and waterjet velocity on spinal cord deflection. The impact of fluid density is investigated by utilizing two fluids with different densities ($\rho_1 \simeq 1000(kg/m^3)$, $\rho_2 \simeq 1160(kg/m^3)$). It is important to note that the temperature variation of the waterjet and specimen during the test is negligible, and, for enhanced accuracy and reliability, the waterjet in this test exclusively interacts with the anterior side of the spinal cord specimens.

For this purpose, the spinal cords of 20 adult sheep (male, ~45-50 kg weight and 2 years old) are divided into 6 pieces (~4 cm long) and fixed without tension in a prepared setup as shown in Figure 3 and Figure 4. A high-speed and high-resolution camera is used to record the deflection in time. The prepared specimens are then tested with nozzles (0.2, 0.3, 0.4, 0.5 mm diameter) at pressures ranging from 1 to 8 bar. The nozzle is held perpendicular to the spinal cord axis (90°) and at a distance of 2 cm from the meningeal layers to avoid waterjet splashes.

Test2:

This test investigates waterjet interaction with spinal cord after dura mater removal. The effect of the waterjet density and the angle between the nozzle and the spinal cord is also studied. For this purpose, spinal cords of 15 adult sheep (male, ~45-50kg weight and 2 years old) are divided into 5 pieces (~5cm long), then by removing dura mater and without pretension held by the fixture shown in Figure 4. The specimens are tested immediately after the dura mater is removed and the waterjet only interacts with the anterior side of the spinal cord specimens in this test. The nozzle is held 2 cm away at 3 different angles to the axis of the spinal cord (30°, 60°, 90°). To determine the depth of the cut, ink (one percent by volume) is added to the water tank. At this stage, the inked waterjet hits the arachnoid mater directly.

3. Results

Test 1:

As mentioned, dura is the toughest layer of meninges and comprised of dense fibrous tissue and stiff enough to protect spinal cord. Waterjet is ricochet after interaction with sample without visible injury in spinal cord. Deflection of spinal cord designated in Figure 5 measured by ImageMeter application and presented in

Table **3** and Table 4 as K and S under tenth second application of waterjet (T1) and five seconds after waterjet is discontinued (T2). These parameters are deliberated in T2 to know plastic deflection 5 seconds after the test. Data of each row of the table is collected after repeating the test three times to improve accuracy and reliability.

Dura mater shows to be stiff enough to protect spinal cord from rupture under waterjet pressure up to 8 bar with applied nozzle caliber. Even though visible damage has not occurred in dura mater in this test**,** it cannot be guaranteed that the internal tissue of the spinal cord is not damaged. As can be seen in

Table **3**, K/Dc is close to 0.3, with this deflection medical investigation is needed to study probable damage to internal tissue of spinal cord to develop a standard threshold for waterjet properties. Also, it is noticeable from

Table **3** that no remarkable plastic deformation remains permanently in spinal cord up to 8 bar pressure. It means, if these temporary deflections do not damage internal tissues of spinal cord, its structure returns to normal shape quickly.

Table 4 that is similar to

Table **3** in output velocity and nozzle diameter (0.5 mm) presents effect of waterjet fluid density on spinal cord deformation. To have the same output velocity, required pressure is obtained from Table 2, as:

$$V = \left(\frac{2*0.158135*P*10^5}{1160}\right)^{0.591086}$$

4

$$P = 0.036677*V^{1.691086}$$

Results of Table 4 in comparison with

Table **3** indicate that fluid density plays an important role in deformation of spinal cord. As density of fluid increases, deflection parameters, K and S, increases.

Test 2:

Since Arachnoid is filled with elastic tissues and collagen in a spider web-like structure [2], waterjet could pass through this layer and penetrate into subarachnoid space. In this case, penetration power of the jet decreases drastically. It is clear that with high intensity waterjet, one would be able to pass pia mater and reaches internal spinal cord soft tissue. The minimum jet velocity required to pass the arachnoid and pia mater may be defined as V_dp. Waterjet with this velocity can penetrate internal spinal cord soft tissue. V_dp values depends on liquid density and nozzle caliber.

Figure 6 and Figure 7 illustrate V_dp of pure water and salt water for different nozzle diameter and angles. V_dp will be decreased by increasing nozzle's diameter and minimizes when nuzzle is held normal to axis of spinal cord (90°). Salt water due to its higher density required lower V-dp for penetration rather than pure water. The resulting values for each column of these figures have been obtained after performing at least three tests.

Figure 8 illustrates cross section of spinal cord to show waterjet penetration versus time for V_dp with two different nozzle calibers (0.2 and o.5 mm). This figure (Figure 8) depicts that damage area and penetration rate increase by increasing nozzle diameter. Waterjet is able to pierce inner soft tissue to the center of spinal cord for V_dp, but soft tissue penetration rate and the volume of degradation depends on nozzle diameter.

When waterjet reaches to the center, spinal cord begins to swell and its diameter increases. To find a better understanding, a longitudinal incision is made along the axis of the spinal cord. Figure 9-a shows Longitudinal section of spinal cord in the direction of incision for V_dp with 0.5 mm nozzle caliber. Cross section of the specimen (A section) with offset with respect to waterjet interaction location (B section) is shown in Figure 9-b.

Waterjet dissection area is black colored and enclosed by red line. Also, waterjet path along spinal cord axis in specified by a red arrow. As shown in Figure 9, inky waterjet, after reaching the center of spinal cord, runs along central canal that contains cerebrospinal fluids. This is due to minimum resistance of this canal against waterjet fluid movement. Swelling of spinal cord during the test confirms this phenomenon.

Comparison of waterjet spread area in subarachnoid space versus time for velocity of 90 percent of V_dp is shown in Figure 10 using 0.2 and 0.5 mm nozzles. For a certain percentage of V_dp, spread rate beneath arachnoid mater and A_o increase as nozzle diameter increases. A_o is the maximum area which inky liquid spread beneath Arachnoid mater and is defined for each nozzle and jet velocity. Scar area of waterjet spread is indicated schematically in Figure 11. As shown in Figure 11, the scar area spreads drastically in early test time and trends to a flat line over time. The trend line gets closer to A_o faster while nozzle's diameter increases.

3. Discussion

One of the major problems for in-vitro experimental investigations is that fresh human specimens are becoming increasingly difficult to obtain, and when they are available, such specimens are required in large quantities in order to overcome the large scattering effect associated with biological variability [21]. To cope with this problem, animal specimens are regularly used. Specifically, animals including sheep, goats, pigs, calves, and dogs are used to model the human spine. Such animal specimens are more readily available [22] and show much better homogeneity than human specimens when selected for breed, sex, age, and weight [23,24]. In particular, sheep are often used as a model for in-vivo studies, such as histomorphology of the intervertebral disc [25-27] and biomechanical efficacy of fusion techniques in the lumbar spine [28]. Sheep spines have also been used in-vitro to study the initial stabilizing effect of spinal implants in the lumbar [29-31] and cervical regions [32]. Wilke shows that sheep and human vertebrae are most similar in the thoracic and lumbar regions [33]. The human spinal cord and meninges also have the same structure as sheep. Zhang et al. developed an in-vivo indentation test method to measure the force and displacement of the indenter on sheep spinal cord with meninges. An equivalent in-vivo Young's modulus of spinal cord with meninges was then obtained [34].

Test 1 was designed to investigate the effects of fluid density and waterjet parameters on spinal cord deflection. Prepared specimens were tested at pressures ranging from 1 to 8 bar using various nozzle diameters (0.2, 0.3, 0.4, and 0.5 mm). The results showed that the dura mater effectively protected the spinal cord from rupture under waterjet pressures up to 8 bar with the used nozzle sizes. Two key parameters, designated as K and S, were used to quantify the deflection of the spinal cord. From a mechanical standpoint, no visible damage or plastic deformation was observed in this study. However, future studies could consider histopathologic examinations to investigate possible minor damage to the internal tissues of the spinal cord. Based on the results of Test 1, medical researchers do not need to test for deformation of the spinal cord in interaction with the waterjet to simulate probable damage. Instead, they can simply use the designated key parameters to induce spinal cord deformation and examine the damage to the internal soft tissues.

In Test 2, the waterjet interacted with the arachnoid directly after the removal of the dura mater. The function of the meninges is to protect the spinal cord from mechanical trauma. The elastic modulus and toughness of the meninges are much higher than those of the white and gray matter tissues [2,34]. It could be assumed that the toughness and stiffness of the spinal cord decreased gradually and uniformly from the surface to the center. The waterjet could only reach the inner soft tissues of the spinal cord if it had enough momentum to pass through both the arachnoid and the pia mater. This velocity was defined as V_dp and depended on fluid density and nozzle caliber. Otherwise, at velocities lower than V_dp, the waterjet could only propagate below the arachnoid mater in the subarachnoid space because its penetrating power was drastically reduced after passing through the arachnoid mater. This is due to the fact that the arachnoid mater is filled with elastic tissue and collagen in a spider web-like structure [2].

The results showed that V_dp was minimized when the nozzle was normal to the spinal cord axis. It was also decreased by increasing the nozzle's diameter and liquid density. Regarding the V_dp values, as the nozzle diameter increased, the degradation volume and penetration rate increased. Moreover, the waterjet liquid ran along the central canal that contains cerebrospinal fluids, after reaching the center of the spinal cord. This canal has minimum resistance against the movement of waterjet fluid. Additionally, for a certain percentage of V_dp, as the nozzle diameter increased from 0.2 to 0.5 mm, the liquid spread rate beneath the Arachnoid mater as well as A_o increased.

4. Conclusion

Dura mater is stiff enough to protect spinal cord from rupture for pressure up to 8 bar with different nozzle calibers and normal direction of the jet. Spinal cord behaves like a purely elastic material in this range of pressure. In this regard three key parameters of deformation in spinal cord are defined. These parameters play the key role in achieving the standard threshold criteria for safe medical operation. Effect of angle between waterjet and spinal cord axis on deflection is also investigated. It should be noted that the maximum deflection takes place when waterjet flow is normal to spinal cord. Results show that interaction of waterjet do not damage the dura mater up to 8 bar pressure. For waterjet velocities greater than V_dp, the waterjet is capable of passing through both the Arachnoid and pia mater, running along the central canal after reaching the center of the spinal cord. For velocities lower than V_dp, it can only spread beneath the Arachnoid mater in the subarachnoid space. When the waterjet velocities are equal to V_dp, the soft tissue penetration rate and the volume of degradation increase as the nozzle diameter increases. Furthermore, for a certain percentage of V_dp, the liquid spread rate beneath the arachnoid mater and increase as the nozzle diameter increases. Increasing the angle between the nozzle and spinal cord axis up to 90 degrees results in a decrease in V_dp. Moreover, V_dp values decrease with increasing fluid density and nozzle diameter.

Refrences

[1] Maton, A., Jean, H., Charles, W.M., et al. “Human biology and health”, 1 ed., Englewood Cliffs, New Jersey, USA: Prentice Hall, ISBN 0-13-981176-1, (1993).

[2] Guertin, PA. “Central pattern generator for locomotion: anatomical, physiological, and pathophysiological considerations”, *frontiers in neurology,* 3, pp. 183 (2013), doi:10.3389/fneur.2012.00183.

[3] Vasković, J., Ventricles, meninges and blood vessels of the brain, Retrieved from KENHUB: https://www.kenhub.com/en/library/anatomy/meninges-of-the-brain-and-spinal-cord. Accessed December 21, (2021).

[4] Benowitz, L. and Yin, Y. “Optic Nerve Regeneration”, *Arch Ophthalmol*, 128(8), pp. 1059-1064 (2010), doi:10.1001/archophthalmol.2010.152.

[5] Setzer, M., Murtagh, R.D., Murtagh, F.R., et al. “Diffusion tensor imaging tractography in patients with intramedullary tumors: comparison with intraoperative findings and value for prediction of tumor resectability”, *J Neurosurg Spine*, 13(3), pp. 371-380 (2010), doi:10.3171/2010.3.SPINE09399.

[6] Ogawa, Y., Nakagawa, A., Takayama, K., et al. “Pulsed laser-induced liquid jet for skull base tumor removal with vascular preservation through the transsphenoidal approach: a clinical investigation”, *Acta Neurochir*, 153(4), pp. 823–830 (2011), doi: 10.1007/s00701-010-0925-x.

[7] Nakagawa, A. “Pulsed Laser-induced Liquid Jet System for Treatment of Sellar and Parasellar Tumors: Safety Evaluation”, *J Neurol Surg A Cent Eur Neurosurg*, 76(6), pp. 473-482 (2015) doi:10.1055/s-0034-1396436.

[8] Endo, T., Takahashi, Y., Nakagawa, A., et al. “Use of Actuator-Driven Pulsed Water Jet in Brain and Spinal Cord Cavernous Malformations Resection”, *Operative Neurosurgery*, 11(3), pp. 394-403 (2015), doi:10.1227/NEU.0000000000000867.

[9] Derakhshan, R. M.T. Ahmadian, M.T. and Firoozbakhsh, K. "Pull-in criteria of a nonclassical microbeam under electric field using homotopy method", *Scientia Iranica*, 25(1), pp. 175-185 (2018). doi: 10.24200/sci.2017.4315

[10] Alamoud, A.H., Baillot, E., Belabbas, C., et al. “Continuous and Pulsed Experiments with Numerical Simulation to Dissect Pituitary Gland Tumour by Using Liquid Jet”, *Engineering Letters*, 25(3), pp. 348-353 (2017).

[11] Kok, A.C., den Dunnen, S., Lambers, K.T., et al. “Feasibility study to determine if microfracture surgery using water jet drilling is potentially safe for talar chondral defects in a caprine model”, *Cartilage*, 13(2), pp. 1627S-1636S (2019), doi:10.1177/1947603519880332

[12] Babaiasl, M., Boccelli, S., Chen, Y., et al. “Predictive mechanics-based model for depth of cut (DOC) of waterjet in soft tissue for waterjet-assisted medical applications”, *Med Biol Eng Comput*, 58, pp. 1845-1872 (2020). https://doi.org/10.1007/s11517-020-02182-0

[13] Babaiasl, M., Yang, F., Chen, Y., et al. “Predicting depth of cut of water-jet in soft tissue simulants based on finite element analysis with the application to fracture-directed water-jet steerable needles”, *In: 2019 International symposium on medical robotics (ISMR). IEEE*, pp. 1–7 (2019)

[14] Babaiasl, M., Yang, F., Swensen, J.P. “Towards water-jet steerable needles”, *In: 2018 7Th IEEE international conference on biomedical robotics and biomechatronics (biorob) IEEE*, pp. 601–608 (2018)

[15] Moradiafrapoli, M., Marston, J. “High-speed video investigation of jet dynamics from narrow orifices for needle-free injection”, *chemical engineering research and design*, 117, pp. 110–121 (2017), doi:10.1016/j.cherd.2016.10.023

[16] Kraaij, G., Loeve, A.J., Dankelman, J. “Water Jet Applicator for Interface Tissue Removal in Minimally Invasive Hip Refixation: Testing the Principle and Design of Prototype”, *Journal of Medical Devices*, 13(2) (2019), doi:10.1115/1.4043293

[17] Liu, Ch., Chen, R., Han, Ch., et al. “Water jet as a novel technique for enamel drilling ex vivo”, *PLoS ONE*, 16(7):e0254787, (2021) doi:10.1371/journal.pone.0254787

[18] Abdou, G. and Atalla, N. “Applying waterjet technology in surgical procedures”, in R Bhatia, K Arai & S Kapoor (eds), Proceedings of the Future Technologies Conference (FTC) 2018 - Volume 1. Advances in Intelligent Systems and Computing, vol. 880, Springer Verlag, pp. 616-625, Future Technologies Conference, FTC 2018, Vancouver, BC, Canada, 11/15/18, (2019) https://doi.org/10.1007/978-3-030-02686-8_46

[19] Derakhshan, R., Ahmadian, M.T., Chizari, M., et al. “Trimming of sheep spinal cord by waterjet; an experimental study”, *Heliyon*, 9(7), e17872, (2023), https://doi.org/10.1016/j.heliyon.2023.e17872.

[20] Haynes, W. “CRC handbook of chemistry and physics”, 94 ed., Florida: Boca Raton, Florida: CRC Press, Taylor & Francis Group, (2013-2014).

[21] Ashman, R.B., Bechtold, J.E., Edwards, W.T., et al. “In vitro spinal arthrodesis implant mechanical testing protocols”, *Journal of Spinal Disorders*, 2(4), pp. 274–281 (1989).

[22] Edmondston, S.J., Singer, K.P., Day, R.E., et al. “Formalin fixation effects on vertebral bone density and failure mechanics: An study of human and sheep vertebrae”, *Clinical Biomechanics*, 9(3), pp. 175-179 (1994), doi: 10.1016/0268-0033(94)90018-3.

[23] Eggli, S., Schläpfer, F., Angst, M., et al. “Biomechanical testing of three newly developed transpedicular multisegmental fixation systems”, *European Spine Journal*, 1(2), pp.109-116 (1992), doi: 10.1007/BF00300937.

[24] Gurwitz, G.S., Dawson, J.M., McNamara, M.J., et al. “Biomechanical analysis of three surgical approaches for lumbar burst fractures using short-segment instrumentation”, *Spine*, 18(8), pp. 977-982 (1993), doi: 10.1097/00007632-199306150-00005. 18, 977-982.

[25] Osti, O.L., Vernon-Roberts, B. and Fraser, R.D. “Anulus tears and intervertebral disc degeneration. An experimental study using an animal model”, *Spine*, 15(8), pp. 762-7 (1990), doi: 10.1097/00007632-199008010-00005.

[26] Moore, R.J., Osti, O.L., Vernon-Roberts, B., et al. “Changes in endplate vascularity after an outer anulus tear in the sheep”, *Spine*, 17(8), pp. 874-8 (1992), doi:10.1097/00007632-199208000-00003.

[27] Gunzburg, R., Fraser, R.D., Moore, R., et al. “An experimental study comparing percutaneous discectomy with chemonucleolysis”, *Spine*, 18(2), pp. 218-226 (1993), doi: 10.1097/00007632-199302000-00008.

[28] Ahlgren, B., Vasavada, A., Brower, R., et al. “Anular incision technique on the strength and multidirectional flexibility of the healing intervertebral disc”, *Spine*, 19(8), pp. 948-954 (1994), doi:10.1097/00007632-199404150-00014.

[29] Slater, R., Nagel, D. and Smith, R.L. “Biochemistry of fusion mass consolidation in the sheep spine”, *Journal of Orthopaedic Research*, 6(1), pp. 138-144 (1988).

[30] Yamamuro, T., Shikata, J. and Okumura, H. “Replacement of the lumbar vertebrae of sheep with ceramic prostheses”, *Journal of Bone and Joint Surgery*, 72(5), pp. 889-93 (1990), doi: 10.1302/0301-620X.72B5.2211778.

[31] Nagel, D.A., Kramers, P.C., Rahn, B.A., et al. “A paradigm of delayed union and nonunion in the lumbosacral joint-A study of motion and bone grafting of the lumbosacral spine in sheep”, *Spine*, 16, pp. 553-559 (1991), doi:10.1097/00007632-199105000-00012.

[32] Vazquez-Seoane, P., Yoo, J., Zou, D., et al. “Interference screw fixation of cervical grafts—A combined in vitro biomechanical and in vivo animal study”, *Spine*, 18(8), pp. 946-954 (1993), doi: 10.1097/00007632-199306150-00002.

[33] Wilke, H.J., Kettler, A., Wenger, K.H., et al. “Anatomy of the sheep spine and its comparison to the human spine”, *Anatomical Record*, 247(4), pp. 542-555 (1997), doi: 10.1002/(SICI)1097-0185(199704)247:4<542:AID-AR13>3.0.CO;2-P.

[34] Zhang, H., Falkner, P. and Cai, Ch. “In-Vivo Indentation Testing of Sheep Spinal Cord with Meninges”, *Mechanics of Biological Systems and Materials*, 6, pp. 99-104 (2016), doi:10.1007/978-3-319-21455-9_11.

R. Derakhshan earned his Ph.D. in Mechanical Engineering from Sharif University of Technology in 2023, showcasing a profound commitment to academic excellence and innovation in the field. His research contributions exemplify a passion for advancing electronic engineering knowledge and technology.

M.T Ahmadian got his PHD from University of Kansas, Lawrence USA,1986. Since then, he worked as assistant professor in the University of Missouri for one year and later on university of Kansas. From 1990 to present joined department of Mechanical Engineering at Sharif University of Technology. He has published over 350 peer reviewed papers in the journals and conferences. He has advised over 15 PHD students and 100 Master students so far**.**

Figures

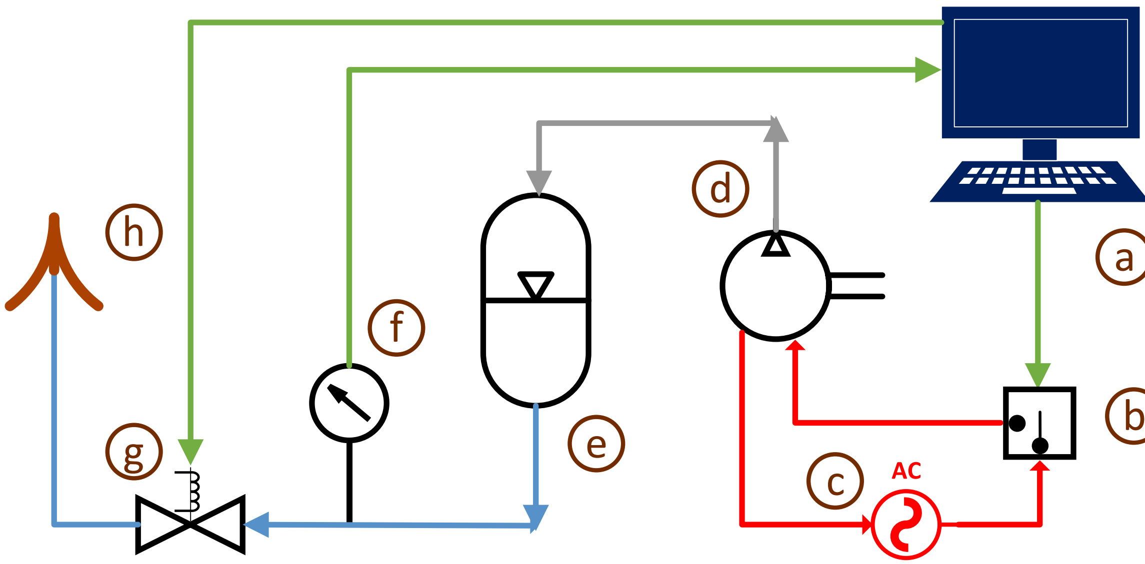

Figure 1

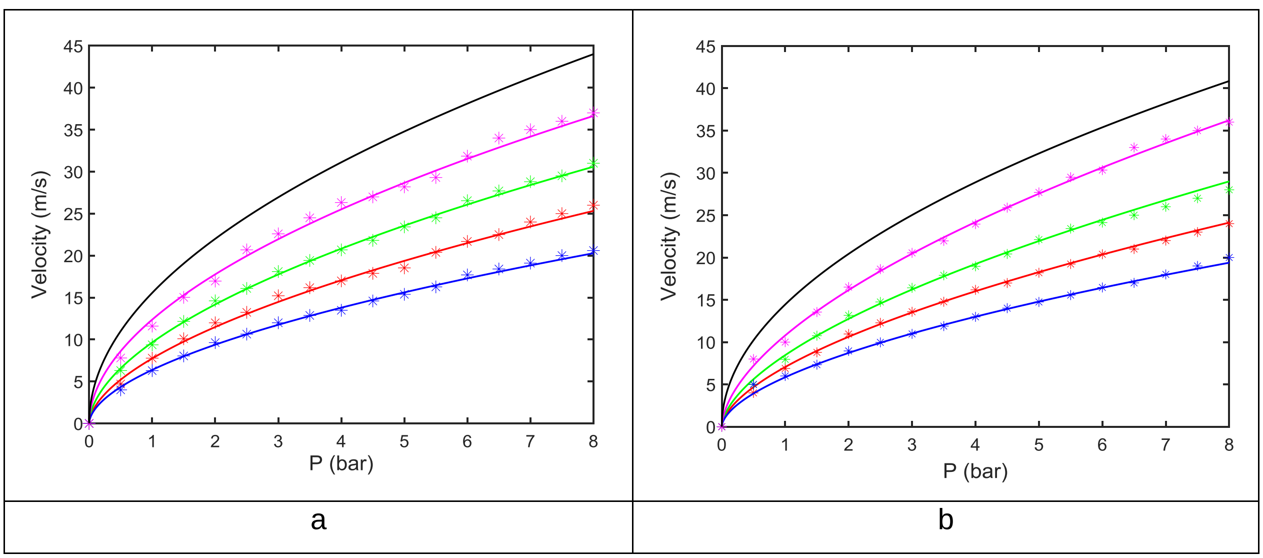

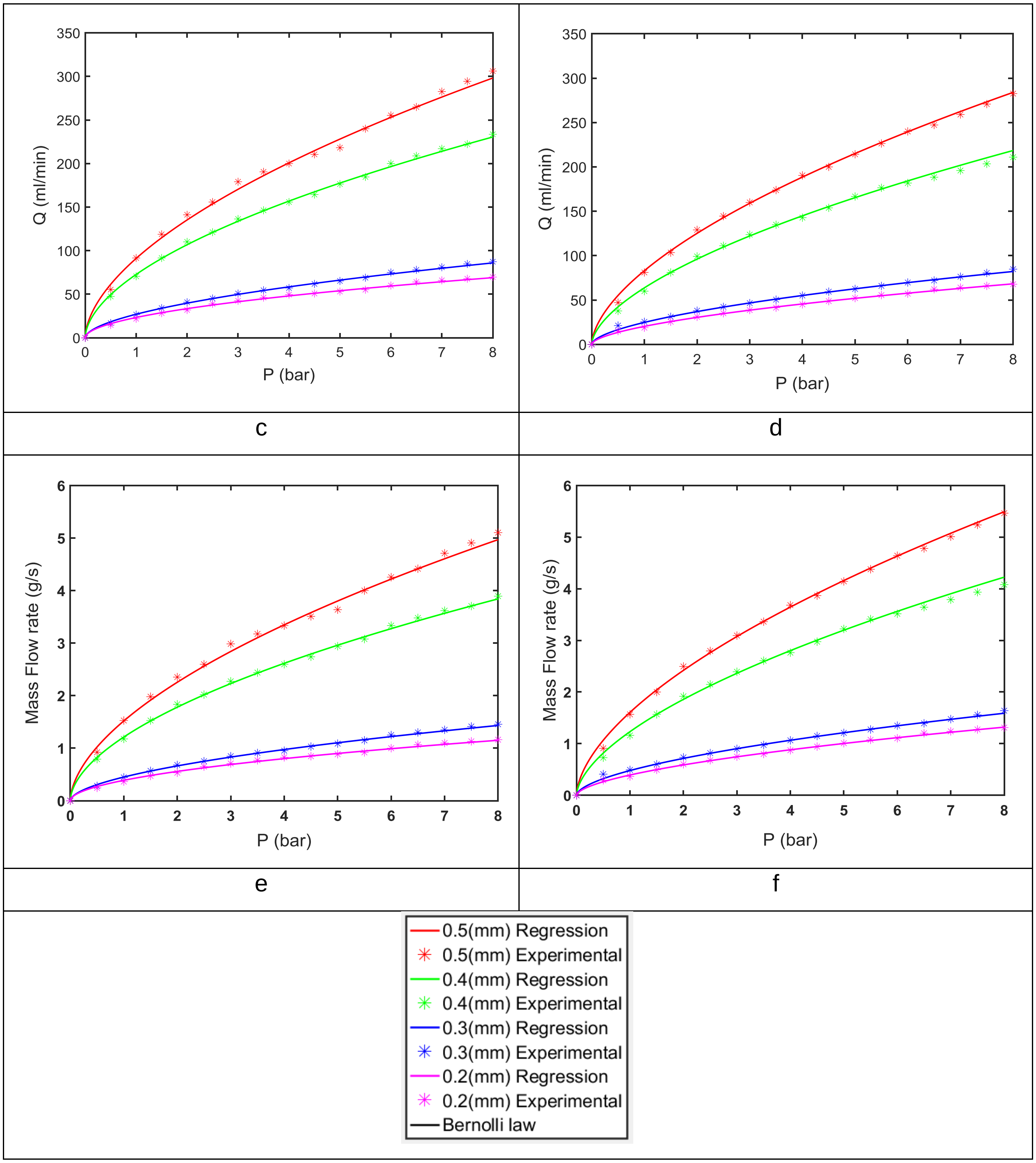
Q (ml/min)
P (bar)
c
d
Mass Flow rate (g/s)
P (bar)
e
f
0.5(mm) Regression
0.5(mm) Experimental
0.4(mm) Regression
0.4(mm) Experimental
0.3(mm) Regression
0.3(mm) Experimental
0.2(mm) Regression
0.2(mm) Experimental
Bernolli law

Figure 2

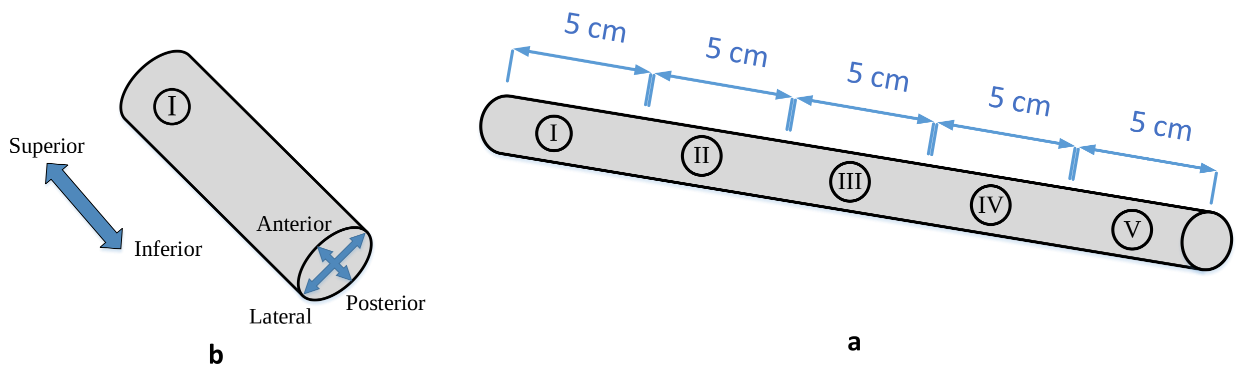

Figure 3

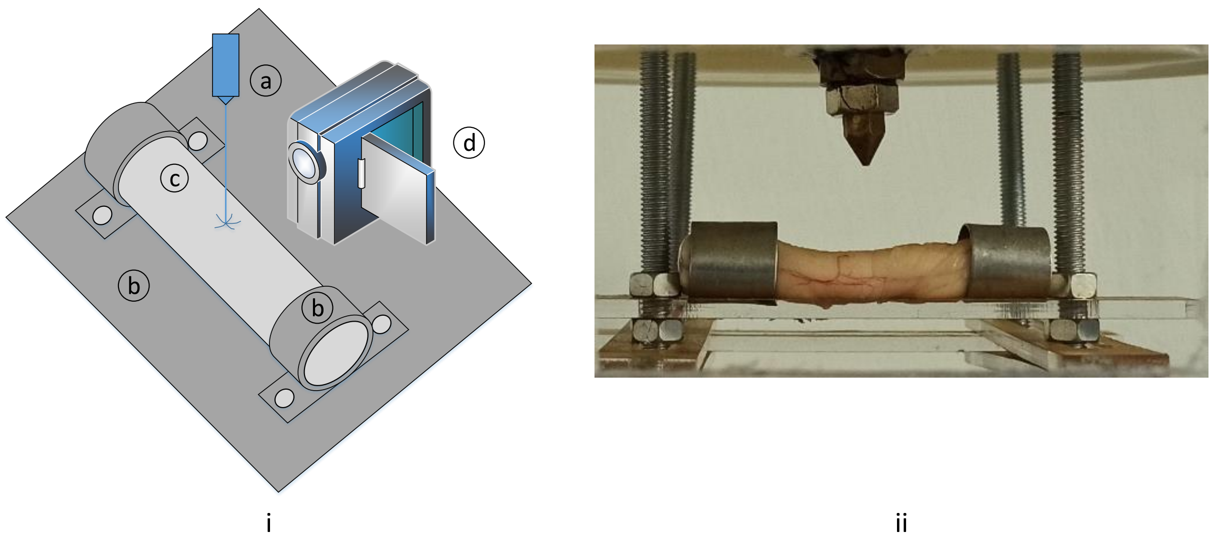

Figure 4

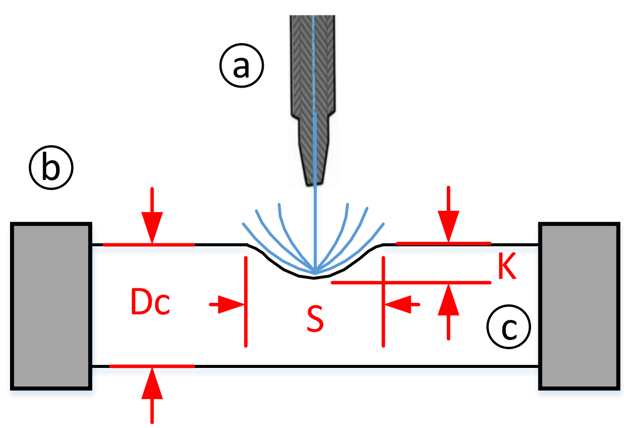

Figure 5

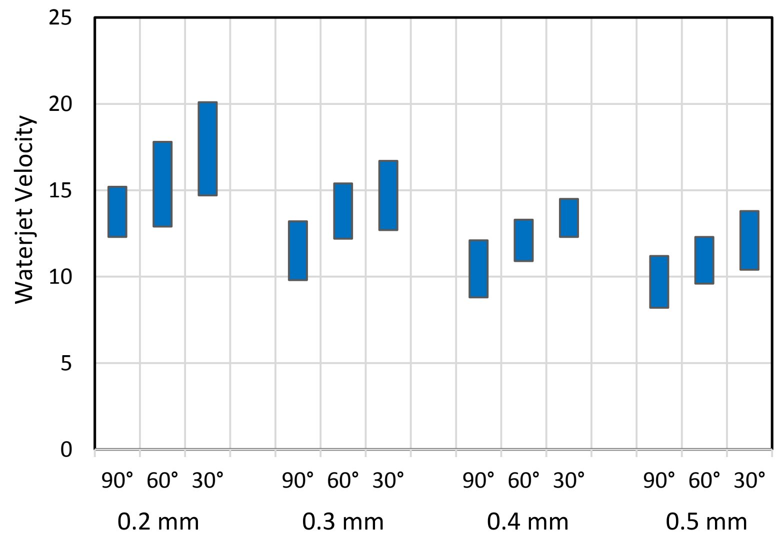

Figure 6

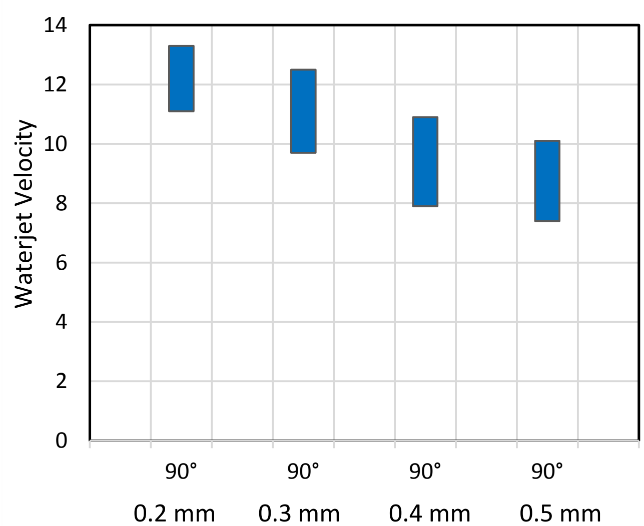

Figure 7

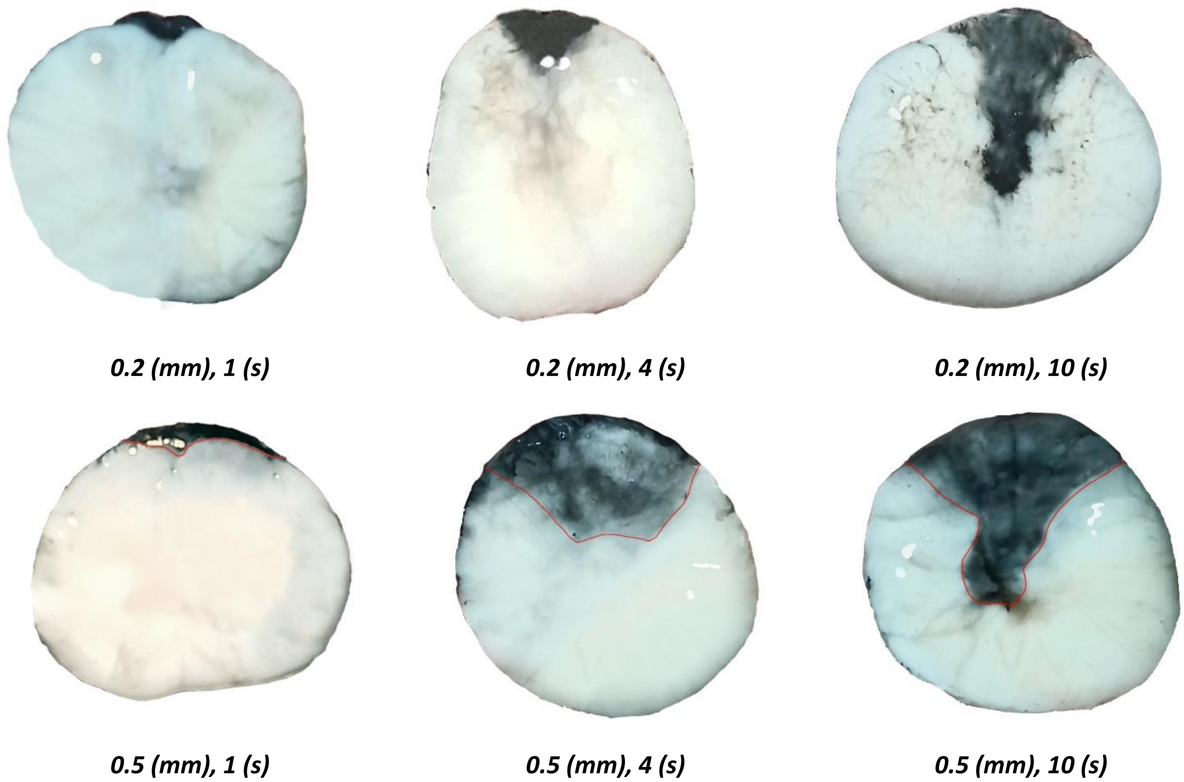

Figure 8

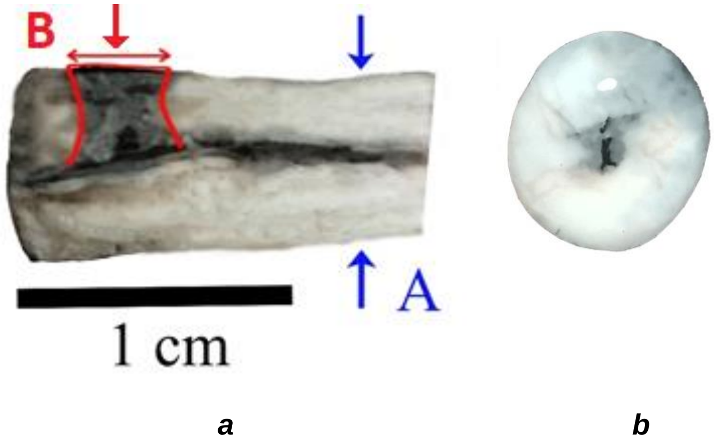

Figure 9

0.2 (mm), 0 (s) *0.2 (mm), 1 (s)* *0.2 (mm), 3 (s)* *0.2 (mm), 7 (s)*

0.5 (mm), 0 (s) *0.5 (mm), 1 (s)* *0.5 (mm), 3 (s)*

Figure 10

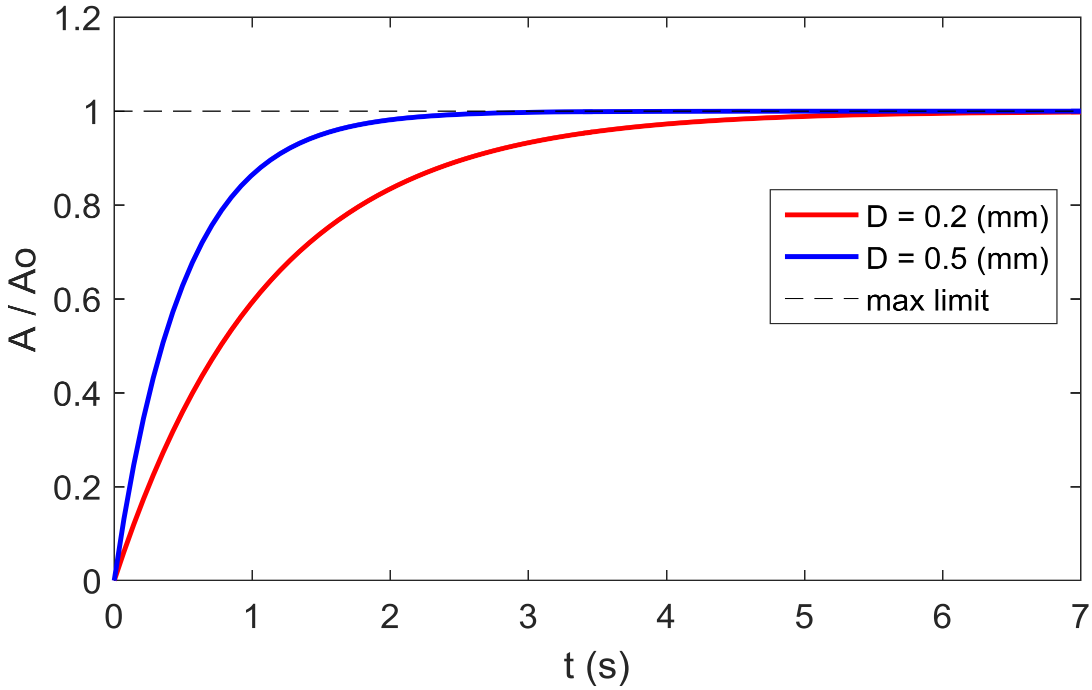

Figure 11

Tables

Table 1

Nozzle caliber (mm)	Regression equation, $P(bar), \rho(kg/m^3), V(m/s)$	Standard Deviation (m/s)
Bernoulli's law	$V = (\frac{2*P*10^5}{\rho})^{0.5}$	——
0.2	$V = (\frac{2*0.617728*P*10^5}{1000})^{0.522187}$	0.664
0.3	$V = (\frac{2*0.139944*P*10^5}{1000})^{0.556161}$	0.255
0.4	$V = (\frac{2*0.297553*P*10^5}{1000})^{0.554777}$	0.302
0.5	$V = (\frac{2*0.181032*P*10^5}{1000})^{0.570084}$	0.442

Table 2

Nozzle caliber (mm)	Regression equation, $P(bar), \rho(kg/m^3), V(m/s)$	Standard Deviation (m/s)
Bernoulli's law	$V = (\frac{2*P*10^5}{\rho})^{0.5}$	——
0.2	$V = (\frac{2*0.343764*P*10^5}{1160})^{0.582587}$	0.423
0.3	$V = (\frac{2*0.124281*P*10^5}{1160})^{0.576281}$	0.326
0.4	$V = (\frac{2*0.213027*P*10^5}{1160})^{0.592478}$	0.484
0.5	$V = (\frac{2*0.158135*P*10^5}{1160})^{0.591086}$	0.242

Table 3

P (bar)	V (m/s)	Parameters	Nozzle Diameter 0.2 mm – Pure Water			
			T1		T2	
			K/Dc	S/Dc	K/Dc	S/Dc
1	**11.6**	Mean	≃ 0	≃ 0	≃ 0	≃ 0
		Stand. deviation	–	–	–	–
2	**16.9**	Mean	≃ 0	≃ 0	≃ 0	≃ 0
		Stand. deviation	–	–	–	–
3	**22.5**	Mean	≃ 0	≃ 0	≃ 0	≃ 0
		Stand. deviation	–	–	–	–
4	**26.3**	Mean	0.050	0.233	≃ 0	≃ 0
		Stand. deviation	0.0056	0.021	–	–
5	**28.1**	Mean	0.055	0.261	≃ 0	≃ 0
		Stand. deviation	0.0385	0.029	–	–
6	**31.8**	Mean	0.061	0.288	≃ 0	≃ 0
		Stand. deviation	0.0043	0.023	–	–
7	**35**	Mean	0.066	0.312	≃ 0	≃ 0
		Stand. deviation	0.0053	0.031	–	–
8	**37**	Mean	0.070	0.323	0.05	0.3
		Stand. deviation	0.0084	0.025	–	–

P (bar)	V (m/s)	Parameters	Nozzle Diameter 0.3 mm – Pure Water			
			T1		T2	
			K/Dc	S/Dc	K/Dc	S/Dc
1	**6.3**	Mean	≃ 0	≃ 0	≃ 0	≃ 0
		Stand. deviation	–	–	–	–
2	**9.6**	Mean	≃ 0	≃ 0	≃ 0	≃ 0
		Stand. deviation	–	–	–	–
3	**12**	Mean	0.051	0.251	≃ 0	≃ 0
		Stand. deviation	0.0031	0.025	–	–
4	**13.5**	Mean	0.060	0.278	≃ 0	≃ 0
		Stand. deviation	0.0054	0.026	–	–
5	**15.4**	Mean	0.067	0.302	≃ 0	≃ 0
		Stand. deviation	0.0053	0.024	–	–
6	**17.7**	Mean	0.075	0.321	≃ 0	≃ 0
		Stand. deviation	0.0056	0.029	–	–
7	**19.1**	Mean	0.081	0.349	≃ 0	≃ 0
		Stand. deviation	0.0089	0.038	–	–
8	**20.6**	Mean	0.088	0.355	0.05	0.3
		Stand. deviation	0.0088	0.032	–	–

P (bar)	V (m/s)	Parameters	Nozzle Diameter 0.4 mm – Pure Water			
			T1		T2	
			K/Dc	S/Dc	K/Dc	S/Dc
1	**9.3**	Mean	0.074	0.341	≃ 0	≃ 0
		Stand. deviation	0.0067	0.037	–	–
2	**14.6**	Mean	0.109	0.453	≃ 0	≃ 0
		Stand. deviation	0.0087	0.041	–	–
3	**18.1**	Mean	0.136	0.556	≃ 0	≃ 0
		Stand. deviation	0.0068	0.044	–	–
4	**20.6**	Mean	0.160	0.644	≃ 0	≃ 0
		Stand. deviation	0.0161	0.071	–	–
5	**23.4**	Mean	0.181	0.727	≃ 0	≃ 0
		Stand. deviation	0.0127	0.073	–	–
6	**26.5**	Mean	0.200	0.805	≃ 0	≃ 0
		Stand. deviation	0.0120	0.072	–	–
7	**28.8**	Mean	0.218	0.871	0.05	0.4
		Stand. deviation	0.0174	0.061	–	–
8	**31**	Mean	0.235	0.923	0.08	0.4
		Stand. deviation	0.0117	0.074	–	–

P (bar)	V (m/s)	Parameters	Nozzle Diameter 0.5 mm – Pure Water			
			T1		T2	
			K/Dc	S/Dc	K/Dc	S/Dc
1	**7.7**	Mean	0.093	0.411	≃ 0	≃ 0
		Stand. deviation	0.0084	0.045	–	–
2	**12**	Mean	0.138	0.562	≃ 0	≃ 0
		Stand. deviation	0.0110	0.051	–	–
3	**15.2**	Mean	0.174	0.714	≃ 0	≃ 0
		Stand. deviation	0.0139	0.057	–	–
4	**17**	Mean	0.205	0.816	≃ 0	≃ 0
		Stand. deviation	0.0143	0.082	–	–
5	**18.5**	Mean	0.232	0.924	≃ 0	≃ 0
		Stand. deviation	0.0234	0.065	–	–
6	**21.6**	Mean	0.258	1.017	0.05	0.3
		Stand. deviation	0.0155	0.081	–	–
7	**24**	Mean	0.282	1.096	0.08	0.4
		Stand. deviation	0.0141	0.098	–	–
8	**26**	Mean	0.304	1.159	0.10	0.4
		Stand. deviation	0.0212	0.116	–	–

Table 4

P (bar)	V (m/s)	Parameters	Nozzle Diameter 0.5 mm – Salt Water			
			T1		T2	
			K/Dc	S/Dc	K/Dc	S/Dc
1.2	**7.7**	Mean	0.095	0.354	≃ 0	≃ 0
		Stand. deviation	0.0059	0.028	–	–
2.5	**12**	Mean	0.145	0.546	≃ 0	≃ 0
		Stand. deviation	0.0115	0.038	–	
3.6	**15.2**	Mean	0.180	0.677	≃ 0	≃ 0
		Stand. deviation	0.0081	0.066	–	–
4.4	**17**	Mean	0.209	0.762	≃ 0	≃ 0
		Stand. deviation	0.0211	0.043	–	–
5.2	**18.5**	Mean	0.234	0.841	0.06	0.3
		Stand. deviation	0.0175	0.098	–	–
6.6	**21.6**	Mean	0.268	0.968	0.09	0.3
		Stand. deviation	0.0146	0.082	–	–
7.9	**24**	Mean	0.297	1.077	0.11	0.4
		Stand. deviation	0.0241	0.061	–	–
9.1	**26**	Mean	0.323	1.171	0.12	0.4
		Stand. deviation	0.0145	0.086	–	–

Figure 1, schematic view of waterjet apparatus

Figure 2, Waterjet velocity calibration on gage pressure for a) pure water and b) saturated saltwater,

Volumetric flow rate of waterjet versus pressure for c) pure water and d) saturated saltwater,

Mass flow rate of waterjet for e) pure water and f) saturated saltwater

Figure 3, specimen sections preparation
a) spinal cord divided to five pieces, b) section I ready to fix in fixture

Figure 4, i) schematic view of specimen held in fixture
a: nozzle, b: fixture, c: specimen, d: camera
ii) specimen held in fixture

Figure 5, defined parameters of test 1, a) nozzle b) fixture, c) specimen

Figure 6, V_dp of nozzles for different nozzle diameter and angles (pure water)

Figure 7, V_dp of nozzles for different nozzle diameter (salt water)

Figure 8, Comparison of waterjet penetration into representative spinal cord specimens versus time for FVT (0.2 and 0.5 mm nozzle)

Figure 9, a) Longitudinal section of a representative spinal cord specimen in the direction of incision for FVT (0.5 mm nozzle), b) cross section of A view

Figure 10, Comparison of waterjet spread beneath the subarachnoid space versus time for 90 percent of FVT (0.2 and 0.5 mm nozzle)

Figure 11, a schematic graph of scar area of waterjet spread beneath the subarachnoid space versus time for 90 percent of FVT (0.2 and 0.5 mm nozzle)

Table 5, Regression equations of waterjet velocity on gage pressure (for pure water $\rho \simeq 1000 kg/m^3$)

Table 6, Regression equations of waterjet velocity on gage pressure (for saturated saltwater $\rho \simeq 1160 kg/m^3$)

Table 7, defined parameters of test 2 with fluid density of $\rho_1 \simeq 1000 (kg/m^3)$, tenth second of test (T1) and five seconds after the test (T2)

Table 8, defined parameters of test 2 with fluid density of $\rho_2 \simeq 1160 (kg/m^3)$, tenth second of test (T1) and five seconds after the test (T2)